JCTC Journal of Chemical Theory and Computation

Letter

pubs.acs.org/JCTC

Introducing the ELF Topological Analysis in the Field of Quasirelativistic Quantum Calculations

Julien Pilmé,*[,†] Eric Renault,[‡] Tahra Ayed,[‡] Gilles Montavon,[§] and Nicolas Galland*[,‡]

[†]Laboratoire de Chimie Théorique, UMR 7616 CNRS, Université Pierre et Marie Curie, Sorbonne Universités, Case Courier 137, 4 place Jussieu, 75252 Paris Cedex 05, France

[‡]CEISAM, UMR CNRS 6230, Université de Nantes, 2 Rue de la Houssinière, BP 92208, 44322 Nantes Cedex 3, France

[§]SUBATECH, UMR CNRS 6457, IN2P3/EMN Nantes/Université de Nantes, 4 rue A. Kastler, BP 20722, 44307 Nantes Cedex 3, France

Supporting Information

ABSTRACT: We present an original formulation of the electron localization function (ELF) in the field of relativistic two-component DFT calculations. Using I_2 and At_2 species as a test set, we show that the ELF analysis is suitable to evaluate the spin−orbit effects on the electronic structure. Beyond these examples, this approach opens up new opportunities for the bonding analysis of large molecular systems involving heavy and superheavy elements.

There is currently a growing interest in using relativistic methods as it has become clear that the study of chemistry involving elements across the entire periodic table requires that relativistic effects are taken into account. The most rigorous approaches are based on the four-component (4c) formalism, derived from the Dirac equation, but they have an intrinsically big computational cost. While there has been considerable progress in reducing the computational effort,[1−4] their use is still limited to small molecules, mostly for benchmarking purposes. Either founded on an exact or an approximate formalism, several alternative two-component (2c) methods have been proposed.[5,6] For a decade, some have benefited of the development of relevant algorithms and codes suitable for practical applications on small to medium chemical systems.[7−9] The 2c methods are notably able to account for spin−orbit (SO) effects. Relativistic effects arise from the high speed of electrons in the vicinity of heavy nuclei. One may distinguish between electron spin-independent (scalar) and spin-dependent effects. Scalar effects are associated with the relativistic mass increase of electrons, finally leading to contraction and energetic stabilization of atomic s and p valence shells and expansion and destabilization of d valence shells. The leading spin-dependent effect is the coupling between electron spin and orbital momentum, which in particular for 5p and 6p elements may be of similar size as scalar relativistic effects. The spin−orbit coupling (SOC) causes energetic and spatial splittings of atomic p, d, and f shells.

It is important to mention that one can do scalar-relativistic (one-component, 1c) calculations with a standard non-relativistic computer code with minimum extra code developments (for example, by use of pseudorelativistic effective core potentials, ECPs, or pseudopotentials, PPs). Hence, the study of scalar relativistic effects on the molecular bonding and structures is well documented and could be traced in the literature over the past decades.[10,11] In contrast, the investigations of SO effects on our pictures of bonding are rather limited, while some major trends have been uncovered. One can mention the case of homonuclear diatomic molecules where SOC mixes states of different symmetries and therefore reduces the bond strength:[11,12] σ bonding orbitals combine with π antibonding orbitals, and π bonding orbitals combine with σ antibonding orbitals. Dramatic changes have been observed in the weights of covalent and ionic forms used to describe the bond of heteronuclear diatomic molecules,[13] due to the SO splitting of atomic p shells. Examples of molecules bearing a heavy atom are also reported for which the hybridization or the valence shell electron pair repulsion (VSEPR) structure is influenced by SOC.[14−20] Jahn−Teller distortion, which lowers the molecular symmetry to increase energy stabilization, could be totally quenched by SO effects, and the energy minimum recovers the full symmetry.

In most of these works, the use of molecular or local symmetry appears central to understanding and interpreting the modifications of nonrelativistic concepts. Furthermore, the study of SO effects inside the chemical bond appears hindered mainly by the exclusive use of molecular orbital (MO) theory and the related Mulliken population analysis.[21] But it is by no means the only one, as discussed by Saue et al. in the context of quantum relativistic computations.[18] Several alternative strategies have been proposed to analyze the breaking and the formation of bonds between atoms: the valence bond theory, the natural bond orbitals and its natural population analysis,[22,23] or the atoms in molecules theory (AIM),[24] which relies on the properties (topology) of the total electron density when atoms interact. More elaborate one-density functions could be used to describe the chemical bond such as the electron localization function (ELF) of Becke and Edgecombe.[25] ELF is indeed a signature of the electronic pairs distribution and, because its topology is a powerful tool for characterizing the bonding schemes,[26] this approach has been intensively used, although the obstacles to the calculation of ELF using *ab initio* correlated

Received: July 2, 2012
Published: August 23, 2012

wave functions have been alleviated only in recent years.[27−30] There is no conceptual objection to using such strategies on complex systems, as opposed to small and/or symmetric model systems, to investigate how SOC modifies chemical concepts. However, the relevant programs in the field of relativistic computations are comparatively at the early stage of development.[8,9,31] It is worth noting that very recently, Schott et al. have shown the usefulness of ELF in the context of quasirelativistic calculations despite the fact that the formulation used for ELF is not documented and only a crude analysis is reported.[32] We first present in this paper an implementation of ELF and its topological analysis in the framework of 2c quantum calculations. We have selected the quasirelativistic spin−orbit density functional theory (SODFT), available in the NWChem programs package,[7] notably due to its ability to perform geometry optimizations (and numerical harmonic vibrational frequency calculations) at moderate computational cost for systems composed of several tens of atoms. Illustrations of the SO effects on the bond representation in closed-shell $X^1\sum_g^+$ I_2 and At_2 species are given in a second step to support the originality of the proposed approach.

THEORY

The SODFT method is particularly attractive due to the expediency of DFT computations and the implicit inclusion of electron correlation effects. It takes advantage furthermore of 2c ECPs and PPs, which replace inner-core electrons and significantly reduce the number of basis functions. The inclusion of spin-dependent terms into the variational treatment of the one-electron operator ensures that scalar relativistic and SO effects are treated on an equal footing. The nonrelativistic formalism operating with Kohn−Sham (KS) orbitals represented by real numbers is extended to a 2c formalism where the DFT wave function is constructed from complex single-particle functions known as (pseudo)spinors, $\varphi_i(\mathbf{r})$. These later are expanded using atom-centered Gaussian basis functions, $\chi_\mu(\mathbf{r})$, the expansion coefficients c_i are complex and determined within the SCF procedure:

$$\varphi_i(\mathbf{r}) = \begin{pmatrix} \varphi_{i\alpha}(\mathbf{r}) \\ \varphi_{i\beta}(\mathbf{r}) \end{pmatrix} = \begin{pmatrix} \sum_\mu c_{i\mu}^\alpha \chi_\mu(\mathbf{r}) \\ \sum_\mu c_{i\mu}^\beta \chi_\mu(\mathbf{r}) \end{pmatrix} \tag{1}$$

The reader can find a more complete coverage of these aspects in refs 33−35. There can be many variations in the form of RECPs and PPs. The small-core ECPnMDF (n = 28 and 60 respectively for I and At atoms) PPs used in this work are expressed in the following form:[36,37]

$$V_{PP}(\mathbf{r}) = -\frac{Z_{eff}}{r} + \sum_{ljk} B_{lj}^k \exp(-\beta_{lj}^k \mathbf{r}^2)\mathbf{P}_{lj} \tag{2}$$

where Z_{eff} is the charge of the inner-core. The sum runs over a Gaussian expansion (index k) of semilocal short-range radial potentials which are different for different orbital angular-momentum quantum numbers l and, for a given l, for the two total one-electron angular-momentum quantum numbers $j = l \pm 1/2$ ($\mathbf{P}_{lj}$ is the projector onto the complete space of functions with angular symmetry l, j around the core under study). The parameters B_{ljk} and β_{ljk} are adjusted so that V_{PP} in 2c valence-only atomic calculations reproduces, as closely as possible, a set of all-electron reference energies. To describe the 25 valence electrons of At and I atoms, we opted for the aug-cc-pVXZ-PP-2c (X = T, Q) basis sets, described in ref 38 for At and assembled from the aug-cc-pVXZ basis set[37] and the 2c extensions[39] for I. The applied DFT methods were the widely used B3LYP hybrid functional[40] and the recently introduced M06-2X meta hybrid functional.[41] Hartree−Fock (HF) calculations were also performed within the SODFT framework (by reducing the exchange-correlation functional in the DFT formalism to the sole HF exact exchange functional).

The original ELF formulation of Becke and Edgecombe was designed for the monodeterminantal wave functions (HF determinant). ELF relies on the Laplacian of the conditional same spin pair probability, and it is usually interpreted as a signature of the electronic-pair distribution.[30,42] A few years later, this formulation was generalized to the DFT theory by Savin and co-workers,[43,44] who have proposed an interpretation in terms of the local excess kinetic energy due to the Pauli repulsion. Thus, ELF (noted $\eta(\mathbf{r})$) can be defined as follows for the closed-shell systems:

$$\eta(\mathbf{r}) = \left[1 + \left(\frac{T_s[\rho(\mathbf{r})] - T_w[\rho(\mathbf{r})]}{\frac{3}{10}(3\pi^2)^{2/3}\rho(\mathbf{r})^{5/3}}\right)^2\right]^{-1} \tag{3}$$

In this formulation, the electron density $\rho(\mathbf{r})$, the kinetic density energy $T_s[\rho(\mathbf{r})] = 1/2\sum_i|\nabla\varphi_i(\mathbf{r})|$, and the von Weizsäcker kinetic energy $T_w[\rho(\mathbf{r})] = 1/8|\nabla\rho(\mathbf{r})|^2/\rho(\mathbf{r})$ are evaluated from the KS orbitals, $\varphi_i(\mathbf{r})$. Using the previous definition of ELF (see eq 3), it is possible to easily extend the formulas to the 2c formalism involved in the SODFT method. The total electron density $\rho(\mathbf{r})$ is defined by summation over occupied 2c spinors (see eq 1), $\varphi_i(\mathbf{r})$:

$$\begin{aligned}\rho(\mathbf{r}) &= \sum_i^{occ} \varphi^*{}_i(\mathbf{r})\,\varphi_i(\mathbf{r}) \\ &= \sum_i^{occ} \varphi^*{}_{i\alpha}(\mathbf{r})\,\varphi_{i\alpha}(\mathbf{r}) + \varphi^*{}_{i\beta}(\mathbf{r})\,\varphi_{i\beta}(\mathbf{r}) \\ &= \sum_\mu \sum_\nu (P_{\mu\nu}^\alpha + P_{\mu\nu}^\beta)\chi_\mu(\mathbf{r})\,\chi_\nu(\mathbf{r})\end{aligned} \tag{4}$$

where $P_{\mu\nu}^\alpha = \sum_i^{occ} c_{i\mu}^\alpha (c_{i\nu}^\alpha)^*$ and $P_{\mu\nu}^\beta = \sum_i^{occ} c_{i\mu}^\beta (c_{i\nu}^\beta)^*$ are the density matrix elements for α and β components, respectively. Although the two components can differ if SOC is taken into account, one may assume for ground state closed-shell species that the spin polarization is small. For practical use, the closed-shell formulation of ELF depending only on the total electron density can be reasonably used.[44] In addition to the electron density, the different quantities appearing in ELF are evaluated from the primitive functions and from the $P_{\mu\nu}^\alpha$ and $P_{\mu\nu}^\beta$ density matrix elements:

$$\begin{aligned}T_s[\rho(\mathbf{r})] = \frac{1}{2}\sum_\mu \sum_\nu (P_{\mu\nu}^\alpha + P_{\mu\nu}^\beta) \\ \left(\frac{\partial\chi_\mu(\mathbf{r})}{\partial x}\frac{\partial\chi_\nu(\mathbf{r})}{\partial x} + \frac{\partial\chi_\mu(\mathbf{r})}{\partial y}\frac{\partial\chi_\nu(\mathbf{r})}{\partial y}\right. \\ \left. + \frac{\partial\chi_\mu(\mathbf{r})}{\partial z}\frac{\partial\chi_\nu(\mathbf{r})}{\partial z}\right)\end{aligned} \tag{5}$$

and

$$T_w[\rho(\mathbf{r})] = \frac{1}{8}\frac{\left(\frac{\partial\rho(\mathbf{r})}{\partial x}\right)^2 + \left(\frac{\partial\rho(\mathbf{r})}{\partial y}\right)^2 + \left(\frac{\partial\rho(\mathbf{r})}{\partial z}\right)^2}{\rho(\mathbf{r})} \quad (6)$$

Within eq 6, for example:

$$\frac{\partial\rho(\mathbf{r})}{\partial x} = \sum_\mu \sum_\nu (P^\alpha_{\mu\nu} + P^\beta_{\mu\nu}) \left(\frac{\partial\chi_\mu(\mathbf{r})}{\partial x}\chi_\nu(\mathbf{r}) + \frac{\partial\chi_\nu(\mathbf{r})}{\partial x}\chi_\mu(\mathbf{r})\right) \quad (7)$$

The ELF topological analysis was proposed several years ago as a bridge between the traditional pictures of the chemical bond derived from the Lewis theory and first principles quantum-mechanical methodologies. Briefly, this method makes possible a partitioning of the physical space into electronic volumes, which is achieved by applying the theory of dynamical systems to the properties of the scalar function. The basins are localized around the maxima of the function and are separated by the zero flux surfaces.[26] The ELF partition associates electron density to core and valence regions, without relying on any orbital concept. Each domain or basin can be presented with a chemical signification, namely, core basins around nuclei and valence basins in the lone-pair and bonding regions. Overall, the spatial distribution of the valence basins closely matches the nonbonding and bonding domains of the VSEPR theory.[45] The basin population is then calculated by integrating the one electron density over the basin volume once the function was partitioned. All the topological analyses presented here were carried out using modified versions of the NWChem and TopMoD09[46,47] program packages. The relevant program files which implement the treatment of 2c wave functions are freely available upon request. The ELF isosurfaces were visualized with the Molekel 4.3 software.[48]

RESULTS

The SODFT method has been successfully used to investigate relativistic effects on molecules containing halogen elements and notably astatine.[49−52] The performances of the 2c-B3LYP calculations in conjunction with the aug-cc-pVTZ-PP-2c basis sets can be checked using Table 1. Calculated spectroscopic constants of $X^1\Sigma_g^+$ I_2 and At_2 species are presented and compared to the results of high level calculations. The mean absolute deviation (MAD) against 4c-B3LYP and 4c-CCSD(T) results on the equilibrium bond lengths, R_e, and the vibrational harmonic frequencies, ω_e, are less than 1% and 3%, respectively. Regarding the predictions of dissociation energies, D_e, our computations are in fairly good agreement with 4c-CCSD(T) results, the MAD being of 2.3% (note that the I_2 dissociation energy is unfortunately unavailable at 4c-B3LYP level of theory). Hence, we are confident that the selected level of theory, 2c-B3LYP/aug-cc-pVTZ-PP-2c, is sufficiently accurate to finely describe the properties of closed-shell I_2 and At_2 species. Note that the validity of the collinear approach (used in the SODFT method) has also been verified in the case of I_2 and At_2: any arbitrary choice of the spin quantization axis in the calculation leaves the total energy unchanged.

Table 1. Spectroscopic Constants (R_e in Å, ω_e in cm^{-1}, and D_e in eV) of I_2 and At_2 Species Calculated at Various Levels of Theory

	I_2			At_2		
	R_e	ω_e	D_e	R_e	ω_e	D_e
2c-B3LYP	2.725	200	1.27	3.048	109	0.65
ΔSO[a]	+0.021	−12	−0.60	+0.167	−44	−1.06
4c-B3LYP[b,c]	2.723	201		3.112	102	0.54
4c-CCSD(T)[d]	2.717	206	1.28	3.046	108	0.63

[a]SO effect is defined as the difference between quasirelativistic and scalar calculated values. [b]Ref 53. [c]Ref 54. [d]Ref 12.

The SO effects on the equilibrium bond lengths, the vibrational harmonic frequencies, and the dissociation energies have been studied by a number of authors.[12,50,55,56] The SOC weakens the bond, and it is especially true for the dimer of astatine where SO splitting between the valence $p_{1/2}$ and $p_{3/2}$ spinors is strongest. Ours results (see Table 1) are in full agreement: R_e lengthens by 5% while ω_e reduces by 41% for At_2. The reduction of the D_e value (1.06 eV) upon SOC is even greater than the dissociation energy itself (0.65 eV). However, this drastic reduction is mainly due to the fact that the D_e value is largely influenced by SO splitting in the atomic asymptote. In other words, the large decrease of I_2 and At_2 dissociation energies mainly comes from the calculations for the open-shell I and At atoms. It comes out that the weakening of the bond is clear, and it can be explained as follows: due to the large relativistic contraction and energetic stabilization, the valence s shell forms an inert pair (often termed the "inert pair" effect). The remaining valence electrons give rise to a $\sigma_g^2\pi_u^4\pi_g^4$ configuration in the scalar relativistic description. The SOC splits the two pairs of π orbitals into their $j_z = \pm1/2$ and $j_z = \pm3/2$ components, and the resultant configuration can formally be written as $\sigma_{1/2\,g}^2\pi_{1/2u}^2\pi_{1/2\,g}^2\pi_{3/2u}^2\pi_{3/2\,g}^2$. Only the occupied $\sigma_{1/2\,g}$ spinor has a net bonding contribution, but SOC leads the spinors with the same j_z quantum number and parity to mix. The $j_z = \pm1/2$ components of the antibonding π_g will mix with the σ_g orbital, which clearly shows that the SO effects weaken the bond.

In what follows, the SO effects on the chemical bond for I_2 and At_2 species were investigated through the ELF topological analysis. Overall, the ELF topology appears split into a chemical picture: core basins, labeled C(X) for an atom X, and valence basins characterized by the number of core basins with which they share a common boundary. This number is called the synaptic order.[57] Nonbonding or monosynaptic basins, labeled V(X), usually correspond to lone pair regions, whereas bonding or disynaptic basins, labeled $V(X_1, X_2)$, characterize the covalent bonds located between the two X atoms. As shown in Figure 1 for At_2, the typical topology of homonuclear X_2 (X = I, At) molecules was found.[58] This yields five basins: two equivalent core basins, $C(X_1)$ and $C(X_2)$; two equivalent valence basins, $V(X_1)$ and $V(X_2)$, accounting for nonbonding density; and one bonding basin, $V(X_1, X_2)$.

The basin populations of these species are presented in Table 2. The topological properties of the bonding basin $V(X_1, X_2)$ deserve special attention because they are crucial to evaluate how the covalent character undergoes a change due to the SO effects. Here, the population of this basin is lower than one electron. Indeed, it was previously shown that such systems have a depleted bonding density since it is strongly delocalized toward lone pairs basins.[58] It is worth noting that the population of $V(I_1, I_2)$ remains twice larger than the one of $V(At_1, At_2)$. This clearly indicates a weaker covalent character for At_2 than for I_2, which is consistent with the calculated R_e, ω_e, and D_e values for the two species (see Table 1). Figure 2

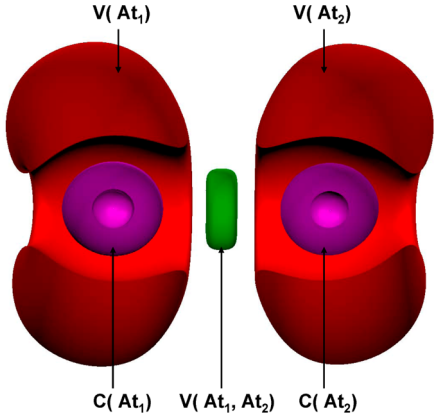

Figure 1. Split of ELF localization domains (isosurface = 0.7) of the At_2 species calculated at the 2c-B3LYP/aug-cc-pVTZ-PP-2c level of theory. Color code: magenta for core C(At) basins, red for valence V(At) basins, and green for the bonding $V(At_1, At_2)$ basin.

Table 2. ELF Population Analysis (electrons) of X_2 Molecules (X = I, At) Obtained at the 2c-B3LYP/aug-cc-pVTZ-PP-2c Level of Theory

	core	valence		
basins	C(X)	V(X)	π^b	$V(X_1, X_2)$
I_2	17.79	6.72	6.50	0.98
ΔSO^a	+0.01	+0.01	+0.25	−0.04
At_2	17.77	6.96	7.66	0.54
ΔSO^a	+0.02	+0.16	+1.52	−0.36

[a]SO effect is defined as the difference between quasirelativistic and scalar calculated values. [b]The π population of the valence basins $V(X_1) + V(X_2)$ is evaluated by taking into account only the expansion coefficients of the p_x and p_y Gaussian basis functions during the integration of the electron density over the basin volumes.

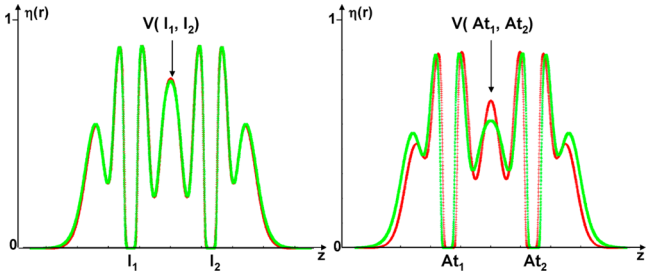

Figure 2. ELF topology of I_2 (left) and At_2 (right) species along the molecular axis. Color code: red for 1c-B3LYP/aug-cc-pVTZ-PP-2c results and green for 2c-B3LYP/aug-cc-pVTZ-PP-2c results.

displays the ELF topologies of I_2 and At_2 species along the molecular axis (z) obtained at scalar and quasirelativistic B3LYP/aug-cc-pVTZ-PP-2c levels of theory. As shown, the ELF topology of I_2 is almost unaffected by the SO effects. This is in agreement with the small modifications predicted for R_e and ω_e when SOC is taken into account (do not forget that the change of D_e value mainly results from SO splitting in the atomic asymptote). The population analysis given in Table 2 supports these findings. Indeed, the basin populations of I_2 remain almost unchanged when the spin-dependent effects are taken into account. For example, the most affected basin, $V(I_1, I_2)$, has its population which decreases from 1.02e to 0.98e. In contrast, the basin populations of At_2 species appear firmly modified when the SOC is accounted for. Indeed, the population of the bonding basin $V(At_1, At_2)$ decreases strongly from 0.90e to 0.54e in favor of the nonbonding V(At) basins. This large decrease must be understood as a patent weakening of the bond covalent character. In addition, the SO effects on the topology of At_2 are clearly visible in Figure 2 (right) where the ELF maximum in the bonding region $V(At_1, At_2)$ appears strongly weakened. It is worth noting that all these results are in full agreement with the rather large modifications of the structural and the energetic properties of At_2 when SOC is taken into account (see Table 1).

In MO theory, the weakening of the bond covalent character is explained by a mixing of the σ_g bonding orbital and the π_g antibonding orbitals due to SOC. As the ELF analysis differs from the orbital concepts, it would be interesting to confront both theories in order to gain a deeper understanding of the chemical bond. We have notably evaluated the π populations because these quantities appear in MO theory correlated to the SO effects on the bond strength. This can be evaluated by taking into account only the coefficients of the p_x and p_y Gaussian basis functions during the integration of the electron density over the basin volumes. While the π populations of the core basins are quasi-unaffected by SO effects, the situation is clearly different for some valence basins. More precisely, the π population for the bonding basins is small (always lower than 0.10e), and its variation is weak. But the SOC markedly increases the π populations of the nonbonding V(X) basins while the total population of the $V(X_1, X_2)$ basin decreases in the same time (see Table 2). Using qualitative orbital language, this phenomenon shall be viewed as an electron withdrawal from the covalent σ bond to the valence π system that is essentially located in the lone-pairs region. It is especially patent for At_2 species where SO splitting between the valence $p_{1/2}$ and $p_{3/2}$ spinors is strongest: a large increase of 1.52e is observed for the π population of the nonbonding V(At) basins. Thus, these results clearly highlight the relationship between the SOC and the π character of the lone pairs, and the resulting effects on the electronic structure of these systems.

The reliability of the uncovered trends via the ELF topological analysis of 2c-B3LYP/aug-cc-pVTZ-PP-2c wave functions have also been checked (see Table S1−S4 in the Supporting Information). Basis set incompleteness effects were evaluated by replacing the aug-cc-pVTZ-PP-2c basis sets, used to describe the 25 valence electrons of At and I atoms, by the much more flexible aug-cc-pVQZ-PP-2c basis sets. Our results appear particularly stable as only minor changes could be noticed. The effects of electron correlation were also tested by performing the ELF topological analysis on 2c wave functions obtained with another DFT functional, M06-2X, and the HF method. Pretty close results are obtained at the 2c-M06-2X/aug-cc-pVTZ-PP-2c level of theory. For instance, a decrease of −0.30e for the population of the bonding basin $V(At_1, At_2)$ has been identified, when the SOC is accounted for, in good agreement with the −0.36e decrease obtained with B3LYP functional and the same basis set. As expected for HF calculations, that does not account for Coulomb correlation, the basin populations differ from populations obtained at the DFT level of theory. However, it is worth noting that similarly to DFT results, a large decrease of population of the At−At bond is clearly observed (−0.22e) in favor of the nonbonding V(At) basins. Furthermore, the ELF topology of I_2 species remains almost unaffected by SO effects at the 2c-HF/aug-cc-pVTZ-PP-2c level of theory, as previously discussed.

The two typical systems studied show that the ELF topological analysis appears suitable to underline the SO effects on the electronic structure. The new formalism introduced allows notably studying molecular systems where the consideration of SOC is crucial. Future works will focus of new applicability of this analysis to a larger panel of species involving heavy elements. The topological analysis of VSEPR distorsions for medium-size systems involving heavy and superheavy elements appears particularly attractive. The implementation of both the distributed electrostatic moments based on the ELF partition (DEMEP)[47] analysis and the AIM topological analysis for relativistic 2c quantum calculations are currently under active development.

■ ASSOCIATED CONTENT

Supporting Information

Four tables reporting spectroscopic constants and ELF population analysis obtained at various levels of theory. This material is available free of charge via the Internet at http://pubs.acs.org.

■ AUTHOR INFORMATION

Corresponding Author

*E-mail: pilme@lct.jussieu.fr, nicolas.galland@univ-nantes.fr.

Notes

The authors declare no competing financial interest.

■ ACKNOWLEDGMENTS

The authors would like to thank the French National Research Agency (ANR 2010-BLAN-0807-01) and the "Region Pays de la Loire" (NUCSAN project) for financial support. This work was performed using HPC resources from GENCI-CINES/IDRIS (Grant 2011-c2011085117) and CCIPL (Centre de Calcul Intensif des Pays de la Loire).

■ REFERENCES

(1) Visscher, L. *Theor. Chem. Acc.* **1997**, *98*, 68−70.
(2) Saue, B. T.; Faegri, K.; Helgaker, T.; Gropen, O. *Mol. Phys.* **1997**, *91*, 937−950.
(3) Nakajima, T.; Hirao, K. *J. Chem. Phys.* **2004**, *121*, 3438−3445.
(4) Belpassi, L.; Tarantelli, F.; Sgamellotti, A.; Quiney, H. M. *Phys. Rev. B* **2008**, *77*, 233403.
(5) Saue, T. *ChemPhysChem* **2011**, *12*, 3077−3094.
(6) Autschbach, J. *J. Chem. Phys.* **2012**, *136*, 150902.
(7) *NWChem, A Computational Chemistry Package for Parallel Computers*, version 5.1.1; Pacific Northwest National Laboratory: Richland, WA, 2008.
(8) *TURBOMOLE*, v6.3; University of Karlsruhe; Forschungszentrum Karlsruhe GmbH; TURBOMOLE GmbH: Karlsruhe, Germany, 2011. http://www.turbomole.com (accessed August 20, 2012).
(9) *ADF*, version 2012; Vrije Universiteit: Amsterdam, The Netherlands, 2012. http://www.scm.com (accessed August 20, 2012).
(10) *Relativistic Electronic Structure Theory, Part 2: Applications*; Schwerdtfeger, P., Ed.; Elsevier B. V.: Amsterdam, The Netherlands, 2004.
(11) Dyall, K. G.; Faegri, K., Jr. *Introduction to Relativistic Quantum Chemistry*; Oxford University Press, Inc.: New York, 2007; pp 453−470.
(12) Visscher, L.; Dyall, K. G. *J. Chem. Phys.* **1996**, *104*, 9040−9046.
(13) Faegri, J. K.; Saue, T. *J. Chem. Phys.* **2001**, *115*, 2456−2464.
(14) Saue, T.; Faegri, K.; Gropen, O. *Chem. Phys. Lett.* **1996**, *263*, 360−366.
(15) Nash, C. S.; Bursten, B. E. *J. Phys. Chem. A* **1999**, *103*, 402−410.
(16) Han, Y.-K.; Lee, Y. S. *J. Phys. Chem. A* **1999**, *103*, 1104−1108.
(17) Dyall, K. G. *J. Phys. Chem. A* **2000**, *104*, 4077−4083.
(18) Dubillard, S.; Rota, J. B.; Saue, T.; Faegri, K. *J. Chem. Phys.* **2006**, *124*, 154307.
(19) Rusakov, A. A.; Rykova, E.; Scuseria, G. E.; Zaitsevskii, A. *J. Chem. Phys.* **2007**, *127*, 164322.
(20) Kim, H.; Choi, Y. J.; Lee, Y. S. *J. Phys. Chem. B* **2008**, *112*, 16021−16029.
(21) Mulliken, R. S. *J. Chem. Phys.* **1955**, *23*, 1833−1840.
(22) Foster, J. P.; Weinhold, F. *J. Am. Chem. Soc.* **1980**, *102*, 7211−7218.
(23) Reed, A. E.; Weinstock, R. B.; Weinhold, F. *J. Chem. Phys.* **1985**, *83*, 735−746.
(24) *Atoms in Molecules: A Quantum Theory*; Bader, R. F. W., Ed.; Oxford University Press: New York, 1994.
(25) Becke, A. D.; Edgecombe, K. E. *J. Chem. Phys.* **1990**, *92*, 5397−5403.
(26) Silvi, B.; Savin, A. *Nature* **1994**, *371*, 683−686.
(27) Matito, E.; Silvi, B.; Duran, M.; Sola, M. *J. Chem. Phys.* **2006**, *125*, 024301.
(28) Piquemal, J. P.; Pilmé, J.; Parisel, O.; Gérard, H.; Fourré, I.; Bergès, J.; Gourlaouen, C.; De La Lande, A.; Van Severen, M. C.; Silvi, B. *Int. J. Quantum Chem.* **2008**, *108*, 1951−1969.
(29) de Courcy, B.; Pedersen, L. G.; Parisel, O.; Gresh, N.; Silvi, B.; Pilmé, J.; Piquemal, J. P. *J. Chem. Theory Comput.* **2010**, *6*, 1048−1063.
(30) Feixas, F.; Matito, E.; Duran, M.; Solà, M.; Silvi, B. *J. Chem. Theory Comput.* **2010**, *6*, 2736−2742.
(31) *DIRAC, a relativistic ab initio electronic structure program*, release DIRAC11. http://dirac.chem.vu.nl (accessed August 20, 2012).
(32) Schott, E.; Zárate, X.; Arratia-Pérez, R. *Polyhedron* **2011**, *30*, 846−850.
(33) Peralta, J. E.; Scuseria, G. E.; Frisch, M. J. *Phys. Rev. B* **2007**, *75*, 125119.
(34) Armbruster, M. K.; Weigend, F.; van Wuellen, C.; Klopper, W. *Phys. Chem. Chem. Phys.* **2008**, *10*, 1748−1756.
(35) Scalmani, G.; Frisch, M. J. *J. Chem. Theory Comput.* **2012**, *8*, 2193−2196.
(36) Peterson, K. A.; Figgen, D.; Goll, E.; Stoll, H.; Dolg, M. *J. Chem. Phys.* **2003**, *119*, 11113−11123.
(37) Peterson, K. A.; Shepler, B. C.; Figgen, D.; Stoll, H. *J. Phys. Chem. A* **2006**, *110*, 13877−13883.
(38) Bischoff, F. A.; Klopper, W. *J. Chem. Phys.* **2010**, *132*, 094108.
(39) Armbruster, M. K.; Klopper, W.; Weigend, F. *Phys. Chem. Chem. Phys.* **2006**, *8*, 4862−4865.
(40) Stephens, P. J.; Devlin, F. J.; Chabalowski, C. F.; Frisch, M. J. *J. Phys. Chem.* **1994**, *98*, 11623−11627.
(41) Zhao, Y.; Truhlar, D. G. *Theor. Chem. Acc.* **2008**, *120*, 215−241.
(42) Silvi, B. *J. Phys. Chem. A* **2003**, *107*, 3081−3085.
(43) Savin, A.; Jepsen, O.; Flad, J.; Andersen, O. K.; Preuss, H.; von Schnering, H. G. *Angew. Chem., Int. Ed. Engl.* **1992**, *31*, 187−188.
(44) Kohout, M.; Savin, A. *Int. J. Quantum Chem.* **1996**, *60*, 875−882.
(45) Gillespie, R. J.; Robinson, E. A. *J. Comput. Chem.* **2007**, *28*, 87−97.
(46) Noury, S.; Krokidis, X.; Fuster, F.; Silvi, B. *Comput. Chem.* **1999**, *23*, 597−604.
(47) Pilmé, J.; Piquemal, J.-P. *J. Comput. Chem.* **2008**, *29*, 1440−1449.
(48) Flukiger, P.; Luthi, H. P.; Portmann, S.; Weber, J.; *Molekel*, version 4.3, University of Geneva: Geneva, Switzerland, 2002.
(49) Choi, Y. J.; Lee, Y. S. *J. Chem. Phys.* **2003**, *119*, 2014−2019.
(50) Cho, W. K.; Choi, Y. J.; Lee, Y. S. *Mol. Phys.* **2005**, *103*, 2117−2122.
(51) Champion, J.; Alliot, C.; Renault, E.; Mokili, B. M.; Cherel, M.; Galland, N.; Montavon, G. *J. Phys. Chem. A* **2010**, *114*, 576−582.
(52) Champion, J.; Seydou, M.; Sabatie-Gogova, A.; Renault, E.; Montavon, G.; Galland, N. *Phys. Chem. Chem. Phys.* **2011**, *13*, 14984−14992.
(53) Fossgaard, O.; Gropen, O.; Valero, M. C.; Saue, T. *J. Chem. Phys.* **2003**, *118*, 10418−10430.
(54) Nakajima, T.; Hirao, K. *J. Chem. Phys.* **2003**, *119*, 4105−4111.
(55) Mitin, A., V.; van Wullen, C. *J. Chem. Phys.* **2006**, *124*, 64305.

(56) Peng, D.; Liu, W.; Xiao, Y.; Cheng, L. *J. Chem. Phys.* **2007**, *127*, 104106.
(57) Savin, A.; Silvi, B.; Colonna, F. *Can. J. Chem.* **1996**, *74*, 1088−1096.
(58) Llusar, R.; Beltrán, A.; Andrés, J.; Noury, S.; Silvi, B. *J. Comput. Chem.* **1999**, *20*, 1517−1526.